Journal of Geophysics and Engineering 2014, vol. 11, article no. 015008
doi:10.1088/1742-2132/11/1/015008

Seismic wave simulation by velocity-stress wave equations in two-phase anisotropic media

Shaohua Zhang [1] , Fan Yang [2] , Duo Xu [3,4] , and Yanghua Wang [4]

[1] Department of Science and Technology, BGP, Zhuozhou, China

[2] College of Geophysics, Chengdu University of Technology, China

[2] Research Institute of Southwest Oil Company, Sinopec, China

[4] Centre for Reservoir Geophysics, Department of Earth Science and Engineering, Imperial College London, UK

Abstract

In two-phase anisotropic media, fast P wave, slow P wave and SV wave are coupled each other. The fast P wavefront shows an elliptical anisotropic feature. Although the wavelet phase of the fast P wavefront in solid and that in fluid are the same, the wavelet phases of the slow P waves are opposite. In cases where there is obvious slow P wave in the wavefield, the slow P wave in fluid is stronger than that in solid. The attenuation mechanism introduced in Biot's theory is of secondary importance for the fast P-wave and the SV wave, but dissipation coefficients have a significant effect to the slow P wave. If there is a large dissipation in the media, the slow P wave will be attenuated very quickly. When the dissipation coefficients have strong anisotropy, the slow P wave is attenuated not just along one direction which has a big dissipation coefficient, but for the entire slow P wavefield. Hence the slow P wave is hardly observable in practice on surface seismic records. It is clearly a limitation with conventional seismic analysis which should be aware in reservoir geophysics.

Key words: anisotropy, Biot theory, dissipation coefficient, two-phase media, wave simulation

1. Introduction

Porous rock consists of solid skeleton and pore space. A theory for wave propagation in poroelastic media was developed by Biot (1962a, b), and was an advanced theory of Biot (1956a, b). The media considered are a general anisotropic poroelastic solid with a viscous fluid saturating its pores of anisotropic permeability. The wave propagation phenomenon in saturated porous media is explained through a relative displacement of fluid particles to the displacement of solid particles (Šrámek *et al*. 2007).

The two-phase anisotropic model is a representative to simplified periodic thin layered media, in which the porous space can be saturated with fluid. Figure 1 shows an outcrop of periodic sedimentary thin beds in the south coast of England. These sand layers have a high porosity of 20% and a high permeability of 200-500 mD. Seismic responses of this stratified porous media both from physics laboratory and numerical simulation would be interest to reservoir geophysics (Masson and Pride 2007, Liu *et al*. 2011, Xu *et al*. 2011). In this paper,

2-D wave equations in two-phase anisotropic media are derived based on generalized Hooke's law and Biot's theory. The wave equations are formed either in displacements or particle velocities and stresses. As land seismic often records the particle velocities, the velocity-stress equations are implemented in this paper with given parameters in both solid skeleton and pore fluid. Simulated wavefields reveal that fast P wave, slow P-wave and SV wave all have an anisotropic feature.

Figure 1. The two-phase anisotropic model is a representative to simplified periodic thin layered media, in which the porous space can be saturated with fluid.

Wave-induced fluid flow in porous media causes seismic attenuation, which occurs at different spatial scales, macroscopic, mesoscopic and microscopic (Pride *et al*. 2004). The attenuation mechanism introduced in Biot's theory is of secondary importance for the fast P-wave and the SV wave. However, dissipation coefficients have a strong effect to the slow P wave. When the dissipation coefficients have strong anisotropy, slow P waves are attenuated not just along one direction which has a big dissipation coefficient, but for the entire slow P wavefield. This observation that the slow P-wave is highly attenuated in porous media saturated by a viscous fluid is consistent with previous publications (Dai *et al*. 1995).

Synthetic experiments reported by Dai *et al*. (1995) indicated that the amplitude variation with offset (AVO) effect caused by the presence of pores might be observed and could be diagnostic of the matrix and fluid parameters. However, because the differences in slow P waves are hardly observable in practice from surface seismic records, it is clearly a limitation of conventional seismic analysis which should be aware in reservoir geophysics, especially in attempting for the anisotropic dissipation coefficients within reservoirs.

2. The velocity-stress equations for two-phase anisotropic media

For the two-phase system formed by solid skeleton and pore fluid, each individual element of stress, strain, displacement and particle velocity can be described in solid phase and fluid phase separately:

(1) The stress tensor in solid phase is $\boldsymbol{\sigma}$, and the effective stress in fluid phase is s.
(2) The strain tensor in solid phase is $\mathbf{e}$, and the strain in fluid phase is ε.
(3) The displacement tensor in solid phase is $\mathbf{u}$, and the displacement tensor in fluid phase

is $\mathbf{U}$.

(4) The particle velocity tensor in solid phase is $\mathbf{v}$, and the particle velocity tensor in fluid phase is $\mathbf{V}$.

Wavefields are often presented as displacements $\mathbf{u}$ and $\mathbf{U}$. This paper simulates wavefields in particle velocities $\mathbf{v}$ in solid phase and $\mathbf{V}$ in fluid phase. The wave equations are coupled with stress $\boldsymbol{\sigma}$ in solid phase and the effective stress s in fluid phase.

According to generalized Hooke's law, a linear stress-strain relationship can be expressed as

$$\begin{bmatrix} \boldsymbol{\sigma} \\ s \end{bmatrix} = \begin{bmatrix} \mathbf{C} & \mathbf{Q} \\ \mathbf{Q}^T & R \end{bmatrix} \begin{bmatrix} \mathbf{e} \\ \varepsilon \end{bmatrix}, \tag{1}$$

where $\mathbf{C}$ is the matrix of elastic constants of the solid phase, R is the elastic parameter of porous fluid, and $\mathbf{Q}$ is a vector of coupling parameters for volume change between solid and fluid.

For two-phase anisotropic media in the x-z space, the stress-strain relationship in solid phase is given by

$$\begin{bmatrix} \sigma_{xx} \\ \sigma_{zz} \\ \sigma_{xz} \end{bmatrix} = \begin{bmatrix} c_{11} & c_{13} & 0 \\ c_{13} & c_{33} & 0 \\ 0 & 0 & c_{55} \end{bmatrix} \begin{bmatrix} \dfrac{\partial u_x}{\partial x} \\ \dfrac{\partial u_z}{\partial z} \\ \dfrac{\partial u_x}{\partial z} + \dfrac{\partial u_z}{\partial x} \end{bmatrix} + \varepsilon \begin{bmatrix} Q_1 \\ Q_3 \\ 0 \end{bmatrix}, \tag{2}$$

(in which the Maxwell relation $c_{31} = c_{13}$ is applied) and that in the fluid phase is given by

$$s = Q_1 \frac{\partial u_x}{\partial x} + Q_3 \frac{\partial u_z}{\partial z} + R\varepsilon, \tag{3}$$

where the fluid strain is

$$\varepsilon = \frac{\partial U_x}{\partial x} + \frac{\partial U_Z}{\partial z}. \tag{4}$$

Equations (2) and (3) may also be expressed in terms of particle velocities as

$$\begin{bmatrix} \dfrac{\partial \sigma_{xx}}{\partial t} \\ \dfrac{\partial \sigma_{zz}}{\partial t} \\ \dfrac{\partial \sigma_{xz}}{\partial t} \end{bmatrix} = \begin{bmatrix} c_{11} & c_{13} & 0 \\ c_{13} & c_{33} & 0 \\ 0 & 0 & c_{55} \end{bmatrix} \begin{bmatrix} \dfrac{\partial v_x}{\partial x} \\ \dfrac{\partial v_z}{\partial z} \\ \dfrac{\partial v_x}{\partial z} + \dfrac{\partial v_z}{\partial x} \end{bmatrix} + \hat{\varepsilon} \begin{bmatrix} Q_1 \\ Q_3 \\ 0 \end{bmatrix}, \tag{5}$$

$$\frac{\partial s}{\partial t} = Q_1 \frac{\partial v_x}{\partial x} + Q_3 \frac{\partial v_z}{\partial z} + R\hat{\varepsilon}, \tag{6}$$

where $\hat{\varepsilon}$ is the first order time differential of the fluid strain ε, and equals to the divergence of particle velocity $\mathbf{V}$ in the fluid phase,

$$\hat{\varepsilon} = \frac{\partial V_x}{\partial x} + \frac{\partial V_z}{\partial z}. \tag{7}$$

In the derivation above, it is assumed that $\{c_{11},\ c_{13},\ c_{33},\ c_{55}\}$ and $\{Q_1,\ Q_3\}$ are constant.

In two-phase anisotropic media, the relationship between stress and displacement in solid phase is given by

$$\nabla \cdot \boldsymbol{\sigma} + \mathbf{f}^s = \frac{\partial^2 (\rho_{11}\mathbf{u} + \rho_{12}\mathbf{U})}{\partial t^2} + \mathbf{B}\frac{\partial(\mathbf{u}-\mathbf{U})}{\partial t}, \tag{8}$$

and that in fluid phase is

$$\nabla s + \mathbf{f}^f = \frac{\partial^2 (\rho_{12}\mathbf{u} + \rho_{22}\mathbf{U})}{\partial t^2} + \mathbf{B}\frac{\partial(\mathbf{U}-\mathbf{u})}{\partial t}, \tag{9}$$

where $\mathbf{f}^s$ and $\mathbf{f}^f$ are the external force vectors acting on the solid and the fluid, respectively, $\{\rho_{11},\ \rho_{12},\ \rho_{22}\}$ are coefficients with density units, and $\mathbf{B}$ is a matrix of dissipation coefficients. Pore fluid flows relative to the solid matrix. Equation (9) is a generalized Darcy's law describing the fluid motion. The term $\mathbf{B}\partial(\mathbf{U}-\mathbf{u})/\partial t$ is the friction force exerted by the fluid on the solid in the direction of motion, as $\partial(\mathbf{U}-\mathbf{u})/\partial t = \partial\mathbf{U}/\partial t - \partial\mathbf{u}/\partial t$ is a relative velocity of the fluid with respect to the solid. In equation (8), this friction force is in the opposite direction.

In equations (8) and (9), the coefficient ρ_{12} represents a mass coupling parameter between fluid and solid (Biot 1956a). When the solid is accelerated, the fluid is restrained so that the average displacement of the fluid is zero. Such a necessary force to prevent fluid displacement is obviously in a direction opposite to the acceleration of the solid, and hence ρ_{12} is negative, $\rho_{12} = -\rho_a$, and ρ_a is a positive-valued apparent mess.

Such an additional apparent mess ρ_a due to fluid should be added to the bulk densities (Biot 1956a) and then coefficients ρ_{11} and ρ_{22} are defined by

$$\begin{aligned} \rho_{11} &= (1-\phi)\rho_s + \rho_a, \\ \rho_{22} &= \phi\rho_f + \rho_a, \end{aligned} \tag{10}$$

where ρ_s is the solid density, ρ_f is the fluid density, and ϕ is the porosity. In equation (10), the mess of solid per unit volume of aggregate is $\rho_{11} + \rho_{12} = (1-\phi)\rho_s$, and the mess of fluid per unit volume of aggregate is $\rho_{12} + \rho_{22} = \phi\rho_f$. Therefore, coefficients $\{\rho_{11},\ \rho_{12},\ \rho_{22}\}$ may be referred to dynamic densities.

Assuming densities $\{\rho_{11},\ \rho_{12},\ \rho_{22}\}$ are constant, equations (8) and (9) may be re-written as

$$\nabla \cdot \boldsymbol{\sigma} + \mathbf{f}^s = \rho_{11}\frac{\partial \mathbf{v}}{\partial t} + \rho_{12}\frac{\partial \mathbf{V}}{\partial t} + \mathbf{B}(\mathbf{v}-\mathbf{V}), \tag{11}$$

$$\nabla s + \mathbf{f}^f = \rho_{12}\frac{\partial \mathbf{v}}{\partial t} + \rho_{22}\frac{\partial \mathbf{V}}{\partial t} - \mathbf{B}(\mathbf{v}-\mathbf{V}), \tag{12}$$

expressed in terms of particle velocities $\mathbf{v}$ and $\mathbf{V}$ in solid and fluid phase, respectively. These two equations (11-12) may be re-arranged to

$$\begin{pmatrix} \partial\mathbf{v}/\partial t \\ \partial\mathbf{V}/\partial t \end{pmatrix} = \begin{pmatrix} -D_{22} & D_{12} \\ D_{12} & -D_{11} \end{pmatrix} \begin{pmatrix} \nabla \cdot \boldsymbol{\sigma} + \mathbf{f}^s - \mathbf{B}(\mathbf{v}-\mathbf{V}) \\ \nabla s + \mathbf{f}^f + \mathbf{B}(\mathbf{v}-\mathbf{V}) \end{pmatrix}, \tag{13}$$

where $\{D_{11},\ D_{12},\ D_{22}\}$ are normalized density-like coefficients $\{\rho_{11},\ \rho_{12},\ \rho_{22}\}$,

$$D_{11}=\frac{\rho_{11}}{\rho_{12}^2-\rho_{11}\rho_{22}},\qquad D_{12}=\frac{\rho_{12}}{\rho_{12}^2-\rho_{11}\rho_{22}},\qquad D_{22}=\frac{\rho_{22}}{\rho_{12}^2-\rho_{11}\rho_{22}}.$$

It leads to

$$\begin{pmatrix}\partial\mathbf{v}/\partial t\\ \partial\mathbf{V}/\partial t\end{pmatrix}=\begin{pmatrix}-D_{22} & D_{12}\\ D_{12} & -D_{11}\end{pmatrix}\begin{pmatrix}\nabla\cdot\boldsymbol{\sigma}-\mathbf{B}(\mathbf{v}-\mathbf{V})\\ \nabla s+\mathbf{B}(\mathbf{v}-\mathbf{V})\end{pmatrix}-\begin{pmatrix}\hat{\mathbf{f}}^s\\ \hat{\mathbf{f}}^f\end{pmatrix},\tag{14}$$

where $\hat{\mathbf{f}}^s$ and $\hat{\mathbf{f}}^f$ are the effective forces, $\hat{\mathbf{f}}^s=D_{22}\mathbf{f}^s-D_{12}\mathbf{f}^f$, $\hat{\mathbf{f}}^f=D_{11}\mathbf{f}^f-D_{12}\mathbf{f}^s$.

Each dissipation coefficient in matrix $\mathbf{B}$ is given by $b_{ij}=\eta\phi^2/\kappa_{ij}$ (Biot 1956a) defined in terms of the fluid viscous coefficient (η), the porosity (ϕ) and the permeability in different directions (κ_{ij}). In this paper, considering two-phase media in the *x*-*z* plane, the dissipation coefficients are defined as

$$B=\begin{bmatrix}b_{11} & 0\\ 0 & b_{33}\end{bmatrix}.\tag{15}$$

In the *x*-*z* plane, divergences $\nabla\cdot\boldsymbol{\sigma}_x=\nabla_x\sigma_{xx}+\nabla_z\sigma_{xz}$, $\nabla\cdot\boldsymbol{\sigma}_z=\nabla_x\sigma_{xz}+\nabla_z\sigma_{zz}$. Thus, the four particle velocity components can be expressed explicitly as the following:

$$\begin{aligned}
\frac{\partial v_x}{\partial t}&=(D_{12}+D_{22})b_{11}(v_x-V_x)+D_{12}\nabla_x s-D_{22}(\nabla_x\sigma_{xx}+\nabla_z\sigma_{xz})-\hat{f}_x^s,\\
\frac{\partial v_z}{\partial t}&=(D_{12}+D_{22})b_{33}(v_z-V_z)+D_{12}\nabla_z s-D_{22}(\nabla_x\sigma_{xz}+\nabla_z\sigma_{zz})-\hat{f}_z^s,\\
\frac{\partial V_x}{\partial t}&=(D_{11}+D_{12})b_{11}(v_x-V_x)-D_{11}\nabla_x s+D_{12}(\nabla_x\sigma_{xx}+\nabla_z\sigma_{xz})-\hat{f}_x^f,\\
\frac{\partial V_z}{\partial t}&=(D_{11}+D_{12})b_{33}(v_x-V_x)-D_{11}\nabla_z s+D_{12}(\nabla_x\sigma_{xz}+\nabla_z\sigma_{zz})-\hat{f}_z^f.
\end{aligned}\tag{16}$$

The four equations in (5-6) and four equations in (16) together form the wave equations for two-phase anisotropic media. When solving the particle velocities $\mathbf{v}$ and $\mathbf{V}$, one simultaneously obtains the stresses $\boldsymbol{\sigma}$ and s.

In the numerical simulation, the forces $\hat{\mathbf{f}}^s$ and $\hat{\mathbf{f}}^f$ are set as the same source wavelet defined by

$$r=e^{-k^2\left[(x-x_0)^2+(z-z_0)^2\right]},\tag{17}$$

with k=0.3, and $\hat{f}_x^s=\hat{f}_z^s=\hat{f}_x^f=\hat{f}_z^f=r$.

The 2D staggered-grid finite-difference method (Madariaga 1976, Virieux 1986, Levander 1988, Graves 1996, Gottschammer and Olsen 2001, Moczo *et al*. 2002) is used in discretization of the eight equations in (5), (6) and (16). The differential accuracies are given by second order in temporal domain and high order (2K, K = 5) in the spatial domain. Time step is 1 ms. For the stability condition and dispersion analysis, readers may refer to O'Brien (2010).

In order to suppress reflections from four sides of the rectangular model, a numerical sponge is used. The sponge is a zone at the edge of the model where the particle velocity amplitude is artificially reduced by multiplying with a factor, which is equal to one at the

inner boundary of the sponge and decreases towards the outer boundary (Cerjan *et al*. 1985, Hall and Wang 2009).

3. The effect of dissipation coefficients

In order to find out the effect of dissipation coefficient to wavefields, a series of models is designed in table 1. The difference among these models is in dissipation coefficients $\{b_{11},\ b_{33}\}$. The size of the models is 3000 × 3000 m^2.

Table 1. Parameters of two-phase anisotropic models (c_{ij}, Q and R unit: $10^9 \cdot \mathrm{kg} \cdot \mathrm{m}^{-1} \cdot \mathrm{s}^{-2}$, density unit: $\mathrm{kg} \cdot \mathrm{m}^{-3}$, dissipation coefficient unit: $\mathrm{Pa} \cdot \mathrm{s} \cdot \mathrm{m}^{-2}$)

Parameters of solid skeleton					Parameters of pore fluid		Coupling parameters		
c_{11}	c_{33}	c_{13}	c_{55}	ρ_{11}	R	ρ_{22}	Q_{11}	Q_{33}	ρ_{12}
26.5	15.5	6.11	4.34	2170	0.33	190	1.14	0.95	–90
Dissipation coefficients									
Model A					$b_{11} = 5,\quad b_{33} = 15$				
Model B					$b_{11} = b_{33} = 1.5\times10^4$				
Model C					$b_{11} = 5,\quad b_{33} = 1.5\times10^4$				

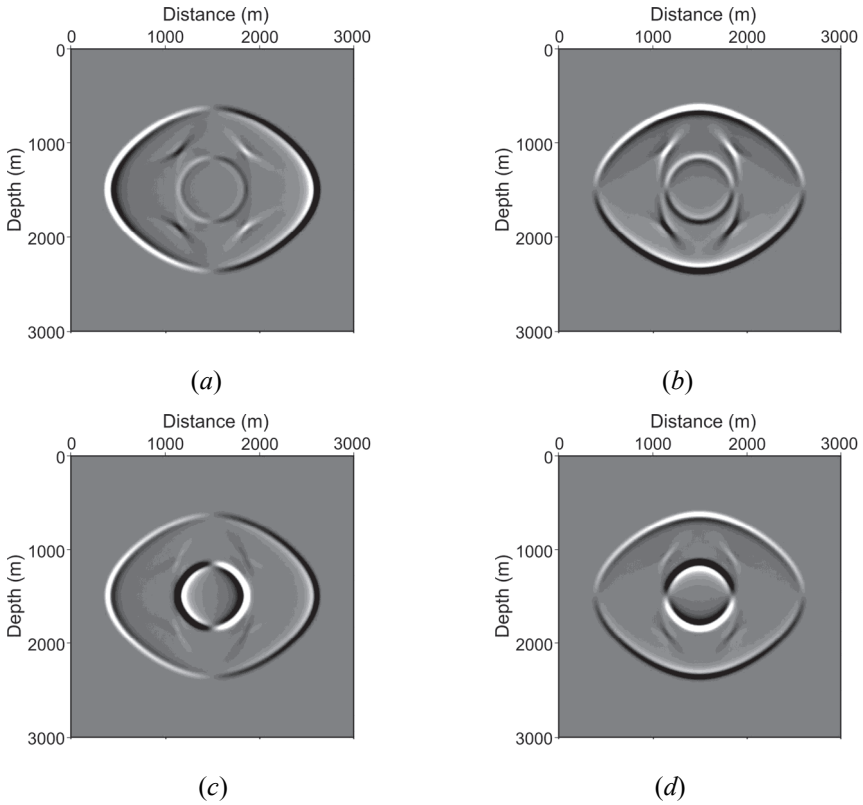

Figure 2. Snapshot of wave propagation (at t = 0.3 s) in model A with small dissipation coefficients. (*a*) Solid phase x component. (*b*) Solid phase z component. (*c*) Fluid phase x component. (*d*) Fluid phase z component.

Model A is designed with small dissipation coefficients in both x and z directions: $b_{11} = 5$ $\mathrm{Pa \cdot s \cdot m^{-2}}$, $b_{33} = 15$ $\mathrm{Pa \cdot s \cdot m^{-2}}$. Figure 2 is the snapshot at $t = 0.3$ s of wave propagation in model A, and shows clearly the fast P wave (with elliptical wavefront), SV wave (with angled wavefront), and slow P wave (a perfect circle) from the outside to the inside. In solid phase (figures a & b), the elliptical fast P wavefront and the angled SV wavefront are easily observed. The amplitudes of fast P wave and SV wave are stronger than they are in fluid phase. Although the phases of fast P wave fronts in solid and in fluid are the same, the phases of slow P waves are opposite. In fluid phase (figures c & d), the slow P wave has stronger amplitude than the fast P wave. It suggests that slow P wave in fluid phase can be easily found.

Model B is designed with strong dissipation. The dissipation coefficients in x and z directions both are $b_{11} = b_{33} = 1.5 \times 10^4$ $\mathrm{Pa \cdot s \cdot m^{-2}}$. Figure 3 is the snapshot at time of 0.3 s. Although the elliptical fast P wavefront and the angled SV wavefront still exist, the slow P wave in solid phase almost disappears (figures a & b). This is because the large dissipation coefficients lead to complete attenuation of the slow P wave in a very short time. Black points in the centre of fluid phase snapshots (figures c & d) are the slow P wave which is also decayed before when it propagates any further.

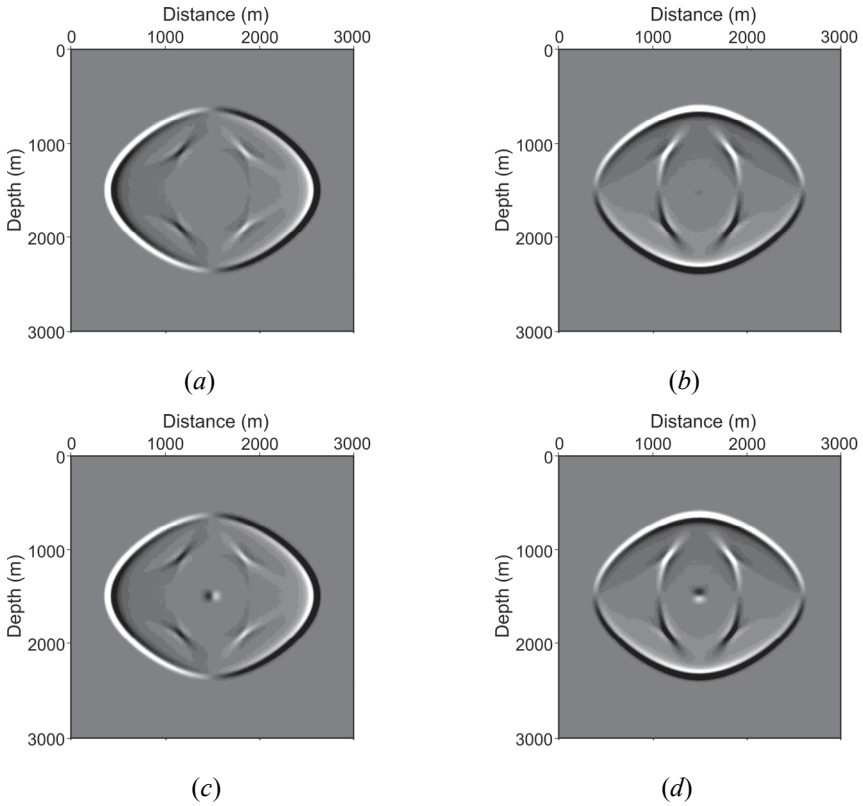

Figure 3. Snapshot of wave propagation (at $t = 0.3$ s) in model B with large dissipation coefficients. (*a*) Solid phase x component. (*b*) Solid phase z component. (*c*) Fluid phase x component. (*d*) Fluid phase z component.

This numerical simulation indicates that the dissipation coefficient is the key factor to cause the attenuation of slow P wave. In fact, the dissipation coefficient in subsurface medium is very large, and hence the slow P wave is attenuated so quickly and cannot be received on

the Earth surface.

Model C is designed with large dissipation coefficient in one direction: $b_{11} = 5 \ \ \mathrm{Pa \cdot s \cdot m^{-2}}$, $b_{33} = 1.5\times10^{4} \ \ \mathrm{Pa \cdot s \cdot m^{-2}}$. Figure 4 is the snapshot (at 0.3 s). It indicates this anisotropy in dissipation coefficients has no much effect on the fast P wave. In solid phase, both the fast P wave and the SV wave have the same wavefront features as that in other two models. For the slow P wave, it is fully attenuated in the *z* direction because of the large dissipation coefficient b_{33}, and is weak also in the *x* direction. This result reveals that when the difference in dissipation coefficient is large in either one direction, the slow P wave is decayed not just along this direction. The most energy of the slow P wave will be attenuated. This indicates that any subsurface anisotropy in dissipation coefficients cannot be observed from the slow P wave.

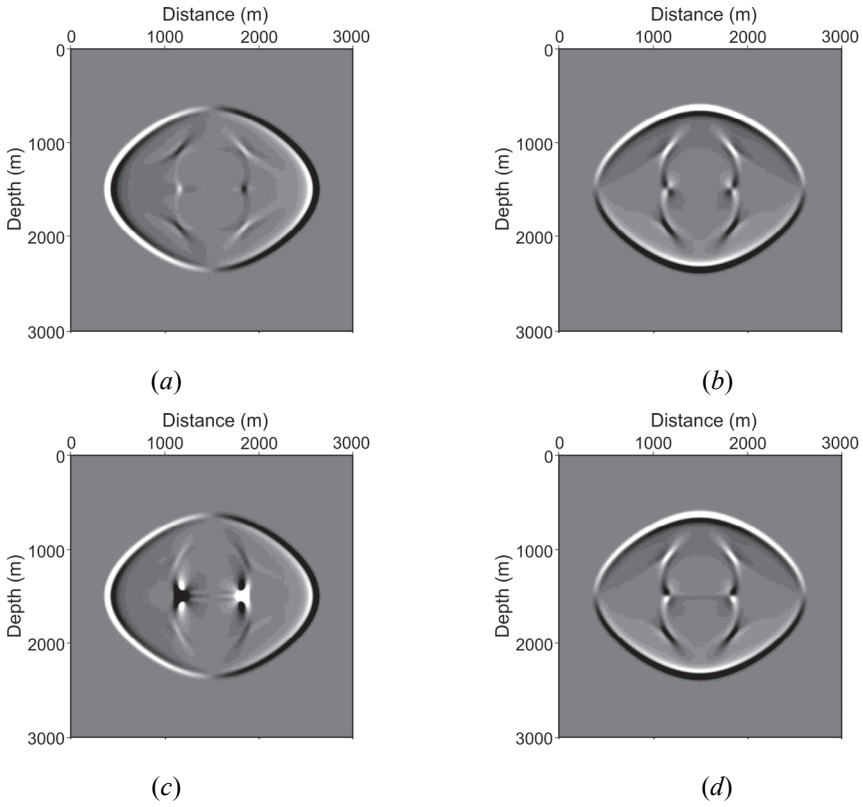

Figure 4. Snapshot of wave propagation (at t = 0.3 s) in model C with anisotropy in dissipation coefficients. (*a*) Solid phase *x* component. (*b*) Solid phase *z* component. (*c*) Fluid phase *x* component. (*d*) Fluid phase *z* component.

Therefore, the effective dissipation can be estimated by $|\mathbf{b}| = \sqrt{b_{11}^2 + b_{33}^2}$. For the slow P wave, the amplitude is $|\mathbf{v}| = \sqrt{v_x^2 + v_z^2}$ in solid phase and $|\mathbf{V}| = \sqrt{V_x^2 + V_z^2}$ in fluid phase. Summing the amplitudes of slow P waves produces $E_{|\mathbf{v}|}$ and $E_{|\mathbf{V}|}$, for a series of $|\mathbf{b}|$, where $b_{11} = b_{33}$ is assumed. Figure 5 plots two curves of normalized amplitude sums $E_{|\mathbf{v}|}(|\mathbf{b}|)$ in sold phase and $E_{|\mathbf{V}|}(|\mathbf{b}|)$ of slow P waves. The horizontal axis is $|\mathbf{b}|$ (in logarithmic scale). Blue curve is the amplitude variation in the solid phase, and the red curve is the amplitude variation in the fluid phase. When the dissipation $|\mathbf{b}| < 100$, the attenuation on the slow P wave is small. For $100 < |\mathbf{b}| < 1500$, there is a linear decay with respect to the logarithmic variation in the dissipation. When $|\mathbf{b}| > 1500$, the slow P wave in the fluid phase is almost completely attenuated.

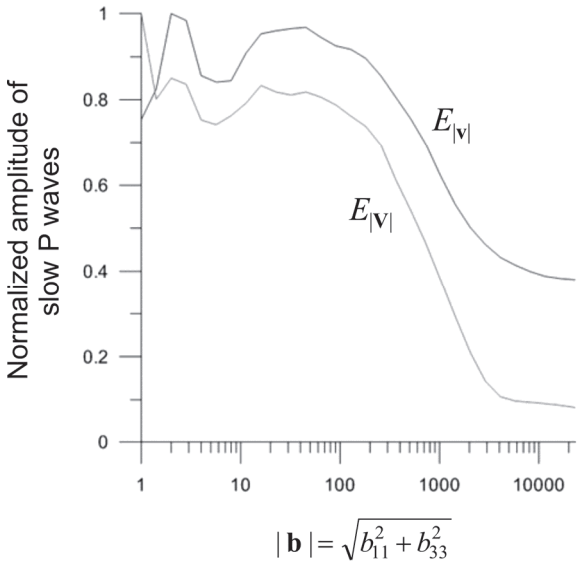

Figure 5. The effects of dissipation coefficients in the solid phase and in the fluid phase. The horizontal axis is the dissipation $|\mathbf{b}|$, and the vertical axis is normalized amplitude sums of slow P waves in sold phase, $E_{|\mathbf{v}|}(|\mathbf{b}|)$, and that in fluid phase, $E_{|\mathbf{V}|}(|\mathbf{b}|)$.

4. Conclusions

The elastic wavefields in two-phase anisotropic media are simulated by using wave equations defined in terms of particle velocity and stress. Numerical results reveal several interesting observations.

(1) The fast P waves in solid and in fluid have the same phase of wavefronts, and both show an elliptical anisotropy feature in the wavefronts.
(2) The phases of slow P wavefronts are opposite in solid and in fluid, because the motion of fluid particle and the motion in the matrix are different in two-phase media.
(3) In an ideal case where there are obvious slow P waves in the wavefields, the slow P waves in fluid phase are stronger than that in the solid phase.
(4) If there is a large dissipation in any direction, the slow P waves will be decayed quickly. This attenuation is occurred not just along one direction with large dissipation coefficient, but on the entire slow P waves.

Thus, the slow P waves are hardly observed from reflection seismic recorded at the Earth surface.

The experiments reveal the influence of the dissipation coefficients in two-phase media. However, governing equations indicate that wavefields also depend upon the other coupling coefficients, such as coupling parameters for volume change between solid and fluid, and the mass coupling coefficient between fluid and solid. Therefore, further investigation will be on their effects, ranging from ‘one-phase’ media with very week coupling to ‘two-phase’ media with strong coupling.

References

Biot M. A., 1956a. Theory of propagation of elastic waves in a fluid-saturated porous solid, I: Low frequency range. *Journal of the Acoustical Society of America*, *28*, 168–178.
Biot M. A., 1956b. Theory of propagation of elastic waves in a fluid-saturated porous solid, II: higher frequency range. *Journal of the Acoustical Society of America*, *28*, 179–191.
Biot M. A., 1962a. Mechanics of deformation and acoustic propagation in porous media. *J. Appl.*

Physics, *33*, 1482–1498.
Biot M. A., 1962b. Generalized theory of acoustic propagation in porous dissipative media. *Journal of the Acoustical Society of America*, *34*, 1254–1264.
Cerjan, C., Kosloff, D., Kosloff, R. & Reshef, M., 1985. A non-reflecting boundary condition for discrete acoustic-wave and elastic-wave equations, *Geophysics*, *50*, 705–708.
Dai N., Vafidis A., and Kanasewich E., 1995. Wave propagation in heterogeneous, porous media: A velocity-stress, finite-difference method. Geophysics, 60, 327–340. doi: 10.1190/1.1443769
Gottschammer E. and Olsen K. B., 2001. Accuracy of the explicit planar free-surface boundary condition implemented in a fourth-order staggered-grid velocity-stress finite-difference scheme. *Bulletin of the Seismological Society of America, 91,* 617–623.
Graves R. W., 1996. Simulating seismic wave propagation in 3D elastic media using staggered-grid finite differences. *Bulletin of the Seismological Society of America*, *86*, 1091–1106.
Hall F., and Wang Y., 2009. Elastic wave modelling by an integrated finite difference method. *Geophysical Journal International*, *177*, 104–114.
Levander A. R. 1988. Four-order finite-difference P-SV seismograms. *Geophysics*, *53*, 1425–1436.
Liu X, Greenhalgh S, and Wang Y, 2011, 2.5-D poroelastic wave modelling in double porosity media. *Geophysical Journal International*, *186*, 1285–1294.
Madariaga R., 1976. Dynamics of an expanding circular fault. *Bull. Seism. Soc. Am., 66*, 639–666.
Masson Y. J., and Pride S. R., 2007, Poroelastic finite difference modeling of seismic attenuation and dispersion due to mesoscopic-scale heterogeneity. Journal of Geophysical Research: Solid Earth, 112(B3), doi: 10.1029/2006JB004592.
Moczo P., Kristek J., Vavrycuk V., Archuleta R. J. and Halada L., 2002. 3D heterogeneous staggered grid finite-difference modeling of seismic motion with volume harmonic and arithmetic averaging of elastic moduli and densities: *Bulletin of the Seismological Society of America, 92*, 3042–3066.
O'Brien G. S., 2010, 3D rotated and standard staggered finite-difference solutions to Biot's poroelastic wave equations: stability condition and dispersion analysis. Geophysics, 75 (4), T111–T119.
Pride S. R. and Berryman J. G., 2003a. Linear dynamics of double-porosity dual-permeability materials I. Governing equations and acoustic attenuation. *Physical Review E*, *68*, paper 036603.
Pride S. R. and Berryman J. G., 2003b. Linear dynamics of double-porosity dual-permeability materials II. Fluid transport equations. *Physical Review E*, *68*, paper 036604.
Pride S. R., Berryman J. G., and Harris J. M., 2004, Seismic attenuation due to wave-induced flow. *Journal of Geophysical Research*, *109*, B01201, pp.19.
Šrámek O., Ricard Y. and Bercovici D, 2007. Simultaneous melting and compaction in deformable two-phase media. *Geophysical Journal International*, *168*, 964–982.
Virieux J., 1986. P-SV wave propagation in heterogeneous medium: velocity-stress finite-difference method. *Geophysics*, *51*, 889–901.
Xu D, Wang Y, Gan Q, and Tang J, 2011, Frequency-dependent seismic reflection coefficient for discriminating gas reservoirs, *Journal of Geophysics and Engineering*, *8*, 508–513.